Available online at www.sciencedirect.com
SCIENCE DIRECT
Catalysis Today 98 (2004) 607–616
CATALYSIS TODAY
www.elsevier.com/locate/cattod

Partial oxidation of methane using a microscale non-equilibrium plasma reactor

Tomohiro Nozaki*, Akinori Hattori, Ken Okazaki

Department of Mechanical and Control Engineering, Tokyo Institute of Technology, 2-12-1 O-okayama, Meguro-ku, Tokyo 152-8552, Japan

Abstract

A flow-type, microscale, non-equilibrium plasma reactor was developed for partial oxidation of methane without a catalyst. A wide range of oxygen and methane mixtures was directly processed without dilution or explosion at ambient temperature because the microscale plasma reactor removes excess heat generated by partial oxidation, thereby maintaining a reaction field at temperatures near room temperature. Consequently, the least reactive methane was excited by high-energy electrons, whereas successive destruction of reactive oxygenates was minimized simultaneously within the extremely confined environment. A highly reactive and quenching environment is thereby obtained within a single reactor: these are paradoxical conditions in conventional thermochemical processes. A major product among liquid oxygenates was methanol, whose selectivity reached 34% at 30% of methane conversion. Selectivity of oxygenates such as methanol and formaldehyde depends strongly on the fragmentation pattern of methane dissociation by electron impact. Maximum selectivity of oxygenates, which is estimated from numerical simulation of a filamentary microdischarge, reaches 60% when the applied electric field corresponds to the breakdown field of methane (80 Td, 1 Td = 10^{-17} V cm^2). The discharge current increases markedly with an applied electric field, but the selectivity of oxygenates decreases as the field strength increases.
© 2004 Elsevier B.V. All rights reserved.

Keywords: Partial oxidation; Methane; Direct methanol synthesis; Non-equilibrium plasma; Microscale plasma reactor

1. Introduction

The great benefit of partial oxidation of methane, particularly direct synthesis of methanol, has attracted substantial effort over the past decade because of increasing demands for energy and environmental protection are incompatible with a modern two-step liquefaction process, which includes energy intensive syngas manufacturing. Nevertheless, yields of organic oxygenates are generally quite low. For instance, one-pass methanol yield is generally no more than 5% [1–3]. More promising results that have claimed a 10% yield (including formaldehyde) have proved difficult to reproduce [4,5]. Periana et al. [6] synthesized a methanol derivative (CH_3OSO_3H) with 70% yield at 220 °C and 3.5 MPa using a platinum catalyst in concentrated H_2SO_4-SO_3. Unfortunately, that process requires large amounts of toxic chemicals, such as H_2SO_4, and 2.5 h reaction time. Bjorklund and Carr [7] reported a 25% methanol yield from a multi-recycling reaction system. However, its one-pass methanol yield could not exceed 4%. One promising solution to achieve a higher yield of useful oxygenates such as methanol is to provide extreme quenching conditions within a single reactor even at elevated temperature and pressure (450–500 °C and 3–6 MPa) to avoid successive destruction of highly reactive oxygenates [3,8,9].

A micro-plasma reactor like those reported herein can satisfy such special requirements that conventional thermochemical processes can not satisfy [10,11]. The principal of generating plasma is similar to dielectric barrier discharge (DBD), which is characterized by a large number of filamentary microdischarges with 1–10 ns duration [12]. Many studies have addressed methane conversion in DBD [13–20]. Larkin et al. [21] performed a comprehensive study on the partial oxidation of methane using a coaxial barrier discharge reactor equipped with a water jacket (2–12 mm gap distance and 688 cm^2 electrode area). Selectivity of

* Corresponding author. Tel.: +81 3 5734 2179; fax: +81 3 5734 2893.
E-mail address: tnozaki@mech.titech.ac.jp (T. Nozaki).

0920-5861/$ – see front matter © 2004 Elsevier B.V. All rights reserved.
doi:10.1016/j.cattod.2004.09.053

oxygenates successfully achieved 60% overall yield. However, that result showed little impact on methanol yield. The one-pass methanol yield was 4% with 30–60 s reaction time because the relatively large reactor space, both radially and laterally, seemed not to restrict further methanol oxidation. This fact emphasizes the necessity for creation of non-equilibrium plasmas within an extremely confined environment. The present study describes the principle of a micro-plasma reactor and application to partial oxidation of methane. Effects of the reactor dimension, O_2/CH_4 ratio, and reaction temperature on low-temperature plasma catalysis of methane are discussed in detail. The reaction mechanism is also discussed based on numerical simulation of micro-discharge formation and emission spectroscopy.

2. Experimental

2.1. Micro-plasma reactor

Fig. 1 shows a micro-plasma reactor. It consists of a Pyrex thin glass tube (i.d. 1.0 mm × 60 mm) and a twisted metallic wire inside the tube (0.2 mm × 100 mm). The reactor is secured in a heat reservoir to maintain a constant reaction temperature. A high-voltage sine wave (2 kV at 75 kHz) is applied between the twisted metallic wire and the grounded heat reservoir. Power consumption by the micro-plasma reactor is between 3 and 10 W; the Lissajous figure method is used for measurement. The principal of generating plasma is similar to DBD, which is characterized by a large number of filamentary microdischarges of 1–10 ns duration. Creation of high-energy electrons activates the least reactive methane at room temperature. Excess gas heating is minimized because of the formation of nanosecond current pulses. Combustion theory dictates that the reactor diameter must be smaller than the quenching diameter of CH_4/O_2 flame to create a highly quenching environment and thereby avoid further oxidation of oxygenates: the quenching diameter is the minimum distance that a flame can propagate through a combustible gas mixture [22]. On the other hand, according to the Paschen's law, the discharge space must be wider than 10 μm to ignite a discharge with moderate applied voltage [23]. These points imply that the glass tube must have an inner diameter of between 10 and 2000 μm at atmospheric pressure. Heat produced by both plasma and partial oxidation is removed with this dimension. Therefore, low-temperature plasma catalysis is maintained even though high methane conversion is achieved. We also used Ni, Mo, and Pt metallic wires, but those results were independent of the metal variety in this experimental configuration. Detailed experimental conditions are shown in Table 1.

Table 1
Experimental conditions

Pressure (kPa)	100
Inner diameter of glass tube (mm)	1, 2[a]
Frequency (kHz)	75
Discharge power (W)	3–10
Total flow rate (sccm)	5, 10, 15, 20
Temperature of heat reservoir (°C)	25, 50, 80, 120, 200
O_2/CH_4 ratio	0[a], 0.2, 0.5, 1.0

[a] Only when measured spectroscopically.

2.2. Gas analysis

Fig. 2 shows the micro-plasma reactor and gas analysis system. A methane and oxygen mixture was fed into micro-plasma reactor. Nitrogen was premixed into the methane cylinder as a reference for gas analysis (10 vol%). We monitored emissions from N_2 (second positive band) and NO (γ-band) [24,25] during plasma processing: N_2 and NO showed no emissions. Chemical reactions involving N_2 or NO_X, which may act as a gaseous catalytic agent, were reasonably negligible. Liquid products such as H_2O, CH_3OH, HCHO, $HCOOCH_3$, HCOOH, and C_2H_5OH were collected using a cold trap (0 °C). The total weight of the liquid mixture was measured after 60–90 min processing. Each component, except H_2O, was then analyzed quantitatively using gas chromatography/mass spectrometry (GC/

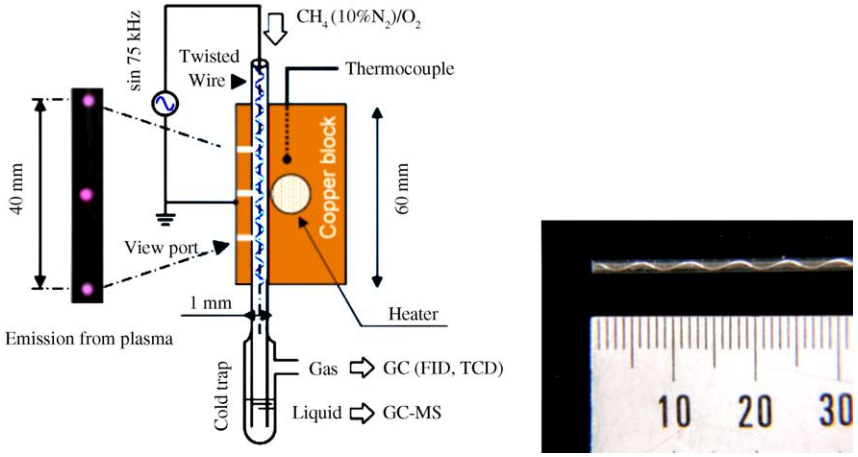

Fig. 1. Micro-plasma reactor apparatus and a photograph of the thin glass tube equipped with a twisted metal wire.

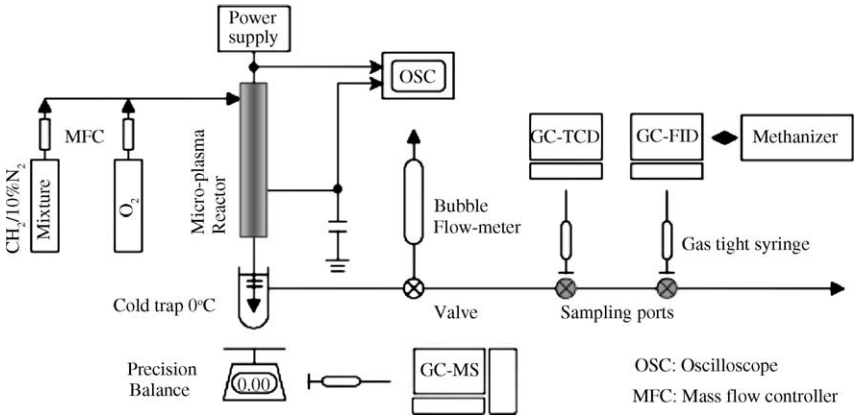

Fig. 2. Micro-plasma reactor and measurement apparatus.

MS; QP-5000, Poraplot Q, carrier gas He, Shimadzu Corp.). CH_4, O_2, N_2, and H_2 were analyzed with a gas chromatograph equipped with a thermal conductivity detector (TCD; GC-8A, molecular sheave 5A, Ar carrier gas; Shimadzu Corp.). CO, CO_2, CH_4, C_2H_6, and C_2H_4 were introduced to the gas chromatograph via a methanizer (FID; GC-8A, Porapack Q, carrier gas N_2; Shimadzu Corp.). We used a gas tight syringe for gas sampling. The syringe was rinsed with acetone, then dried by air blowing before gas sampling. A one-pass yield is described as products generated without recycling and separation of initial feedstock. Methane conversion, product selectivity, and yield are defined as follows.

$$\%\text{conversion of } CH_4 = \frac{CH_4|_{\text{inlet}} - CH_4|_{\text{outlet}}}{CH_4|_{\text{inlet}}} \times 100 \quad (1)$$

$$\%\text{selectivity to } CH_3OH = \frac{CH_3OH|_{\text{outlet}}}{CH_4|_{\text{inlet}} - CH_4|_{\text{outlet}}} \times 100 \quad (2)$$

$$\%\text{selectivity to } H_2 = \frac{0.5 \times H_2|_{\text{outlet}}}{CH_4|_{\text{inlet}} - CH_4|_{\text{outlet}}} \times 100 \quad (3)$$

$$\%\text{yield} = \text{selectivity} \times \%CH_4 \text{ conversion} \quad (4)$$

The amount of water was estimated from the carbon balance, O_2 conversion, and H_2 yield. Those results were compared to the total weight of liquid products and changes in total gas flow for consistency. The carbon balance was consistent within 10% error throughout the experiment. If O_2/CH_4 ratio decreased much below 0.5, yellowish compounds formed on the reactor wall; in addition, the carbon balance decreased below 90%. Methane tended to polymerize under the lack of oxygen. Nevertheless, we observed no soot formation.

3. Principle of microscale non-equilibrium plasma reactor

The principal of generating plasma is similar to DBD. A peculiarity of DBD is the presence of a dielectric insulator on one or both metallic electrodes, which leads to a large number of filamentary microdischarges of nanosecond duration. Fig. 3 shows voltage and current waveforms observed in DBD. The number of nanosecond current pulses is observed at every half cycle of applied voltage. Fig. 4 shows a photograph of a single microdischarge taken with a high-speed intensified CCD camera (i-Star DH712; Andor Technology). Individual filamentary discharge is characterized as weakly ionized plasma with properties resembling transient high-pressure glow discharge. In fact, it consists of an intense cathode spot, which may represent cathode fall, and a filament body, which resembles a positive column. The immediate termination of developing microdischarge caused by the charge that is built up on dielectric material creates a highly reactive non-equilibrium conditions at ambient temperature and atmospheric pressure without extreme gas heating. Fig. 5(a) shows a computer generated streak image of the electron production rate of microdischarge. A detailed description of the simulation model has been described elsewhere [15]. A microdischarge initiates from a tiny plasma spot that is located immediately in front of the metallic cathode. The discharge reaches the dielectric anode in 3.5 ns as it accelerates. Ionization occurs only in an advancing streamer front, where the ionization rate becomes as high as 10^{32} electrons cm^{-3} ns^{-1}. When a streamer bridges the gas gap, it is terminated immediately: ionization ceases. In addition, no ionization occurs in the filament body. Fig. 5(b) shows the CH_3 radical production

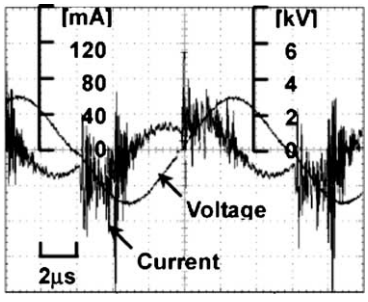

Fig. 3. Voltage and current waveforms.

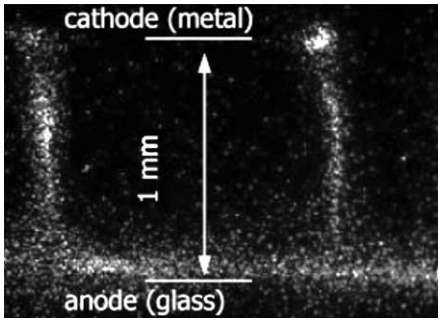

Fig. 4. Photograph of a single streamer produced in pure methane: 10 ns exposure (Pyrex glass: 1 mm).

rate. CH_3 is produced over a slightly wider area than that of electrons because the excitation threshold of CH_3 (9 eV) is lower than the threshold of ionization (12.6 eV, 14.3 eV). Production of radical species in a single streamer is limited in time (ca. 3.5 ns) and in space (near the streamer head). Nevertheless, a relatively large amount of methane is converted because numerous microdischarges are generated, as shown in the current waveform (Fig. 3).

4. Results and discussion

4.1. General aspects of partial oxidation of methane

Table 2 shows oxidative products in terms of reaction temperature with the initial oxygen content of $O_2/CH_4 = 0.5$ (a–d). At low temperatures, where thermal reactions are negligibly small, methane conversion is determined by specific input energy, i.e. W/Q (kJ/l).

$$\text{Methane conversion} \propto \frac{W}{Q} = \frac{V}{Q} \times \frac{W}{V} = (\tau \times f) \times \left(\frac{E}{V}\right)\left(\frac{\text{kJ}}{\text{l}}\right) \quad (5)$$

In this equation, $W = E \times f$ represents input power (W), where f is the operating frequency (s^{-1}); E, the discharge energy per cycle (J); Q, the total gas flow (l/s); V, the reactor volume (liter); and $\tau = V/Q$ for residence time (s). The residence time was calculated from the ratio between total gas flow rate and reactor volume. The micro-plasma reactor does not have sufficient free space inside the reactor to allow induction of secondary flow [26]. The recycling gas flow within thin glass tube (i.d. 1 mm) could be negligible. Methane conversion is clearly independent of the reaction temperature. The operating frequency induces the crucial effect of achieving high methane conversion in a miniaturized reactor within a reasonable time. The one-pass methanol yield reached higher than 10% at 25 °C; it decreased with reaction temperature. Liquid products, including water vapor, were condensed immediately on the reactor wall, and removed from the oxidizing plasma region, preventing the destruction of methanol by electron impact or thermal decomposition. This effect emphasizes the necessity for low temperature synthesis within an extremely confined environment. We propose that high-pressure synthesis between 3 and 6 MPa would improve methanol yield to a greater degree than further miniaturization. High-pressure synthesis is desirable for methanol synthesis from an equilibrium perspective. The high-pressure situation also enhances quenching in the gas phase molecular collisions. Changes in the boiling and melting points of the methanol solution may allow a wide range of reaction temperatures, including temperatures below zero.

Oxygen conversion is also related to Eq. (5). This situation poses a more critical issue for methane conversion and selectivity of oxygenates. Rows a, e, and f in Table 2 portray different residence times. Methane conversion simply increases with reaction time. If oxygen is entirely consumed, methane conversion stops and all oxygenates begin to decompose. Non-equilibrium plasma must exist to trigger the process at room temperature, but effective methane excitation that engenders various oxygenates was achieved only in the presence of oxygen. If oxygen was totally consumed, its main products were CO, CO_2, and H_2O. The same is true when the initial oxygen content was excessively high (h). In these cases, 65% of hydrogen, which comes from methane, becomes H_2O. Active ionic oxygen

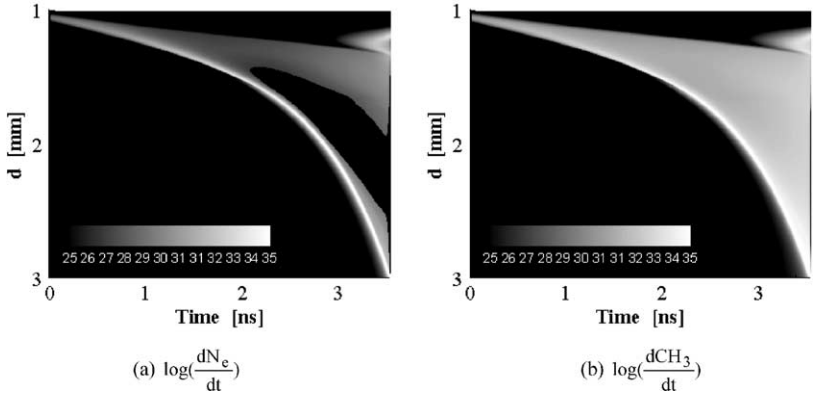

Fig. 5. Streak images of electron and CH_3 production rates ($cm^{-3}\ ns^{-1}$) in pure methane at 300 K and 100 kPa with a metallic cathode ($d = 1$ mm) and a dielectric anode ($d = 3$ mm). The applied electric field is 200 Td, the dielectric constant is 5, and the thickness is 1.0 mm.

Table 2
Effect of reaction temperature and residence time on product yield

	Conditions				% Conversion		% Yield									SEI[a]
	O_2/CH_4	Time (s)	Flow (sccm)	Temp (°C)	CH_4	O_2	CH_3OH	HCHO	HCOOH	CO	CO_2	C_2H_4 /C_2H_2	C_2H_6	H_2	H_2O	kJ/liter
a	0.5	0.28	10	25	45	83	17	3	9	7	4	1	0	3	14	30
b				50	41	91	8	2	3	17	8	1	1	7	21	
c				80	39	94	4	0	1	22	9	1	1	9	24	
d				120	35	82	4	1	1	20	7	1	1	8	21	
e	0.5	0.14	20	25	19	38	4	3	2	6	3	1	0	4	8	15
f		0.57	5		50	100	2	3	1	25	15	1	3	15	28	60
g	0.1	0.14	20	25	16	70	1	1	1	6	3	2	1	5	6	15
h	1.0				15	19	0	0	0	9	5	1	0	5	9	

The discharge power was adjusted to 5 W. Yield of H_2O was estimated from the carbon balance, O_2 conversion, and H_2 yield.
[a] SEI: specific energy input.

species such as O^-, O_2^-, and O_2^{2-} are believed to initiate dissociation of alkanes' C–H bonds [3,27]. In addition, atomic oxygen radicals such as O(3p) and O(1d) are recognized as important radical species in discharge chemistry, especially in ozone production, whereas detailed chemistry involving atomic oxygen has rarely been discussed in conventional thermochemical reaction systems, probably because unusual techniques, such as photo irradiation, are required to produce those radicals. Along with dissociative excitation by electron impact, production of ionic and atomic oxygen species must play an important role in moderate oxidation of methane in low-temperature reactive plasmas where electron impact provides copious amounts of those radicals. Detailed mechanistic studies that involve labeled molecules with isotopic atoms are possible [28,29], but they are beyond the scope of the present study.

4.2. Methane conversion and selectivity of oxygenates

Fig. 6 shows one-pass methane conversion and selectivity of organic oxygenates (liquid products) for all experiments. Results are compared for three different types of thermochemical methods [5,7,30] and DBD [21]. Reaction conditions in thermochemical methods were 300–600 °C and 0.1–6 MPa. High pressure seems to yield higher methanol selectivity. However, methane conversion does not exceed 10%. In addition, oxygen concentration must be as low as possible to minimize further oxidation of oxygenates ($O_2/CH_4 < 0.1$). On the other hand, methane conversion in DBD will reach 40% at ambient temperature because high-energy electron impact will initiate partial oxidation of methane almost independently of temperature and pressure. Methane and oxygen conversion are shown in Fig. 7. Methane conversion depends mainly on how much discharge power would go through the reactor (see Eq. (5)). More than 40% of the methane can be converted by increasing discharge power. Nevertheless, such an effort would be meaningless in a practical sense because oxygen would be used up when methane conversion reaches 40%. The same is true for a thermochemical reaction system. Oxygen conversion reaches 100% at a much lower methane conversion than that of DBD because the initial oxygen concentration is quite low. Maximum methane conversion is limited by 10% unless the initial oxygen amount is increased. Multiple recycling of the remaining feedstock is a reasonable method to increase the

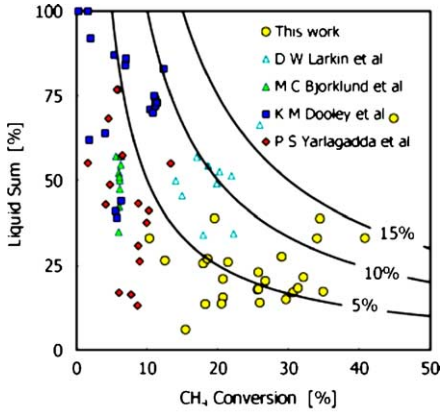

Fig. 6. Methane conversion vs. selectivity of oxygenates. DBD: this work and Larkin et al. [21] (1 atm—room temp., $CH_4/O_2/CO_2$, 30% of liquid oxygenate corresponds to methanol), thermal reaction: Bjorklund and Carr [7] (470–550 °C and 17–100 atm, CH_4/O_2/He, 95% of liquid oxygenate corresponds to methanol), Dooley and co-workers [5] (300–400 °C and 10 atm–70 atm, CH_4/O_2, a liquid oxygenate equals methanol), and Yarlagadda et al [30]. (400–450 °C and 25 atm–65 atm, CH_4/O_2, a liquid oxygenate equals methanol).

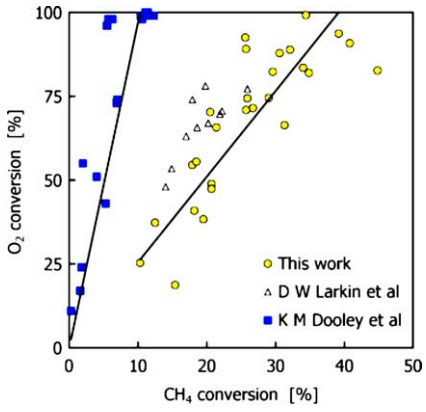

Fig. 7. Relationship between methane and oxygen conversion. DBD: this work and Larkin et al. [21], thermal reaction: Dooley and co-workers [5].

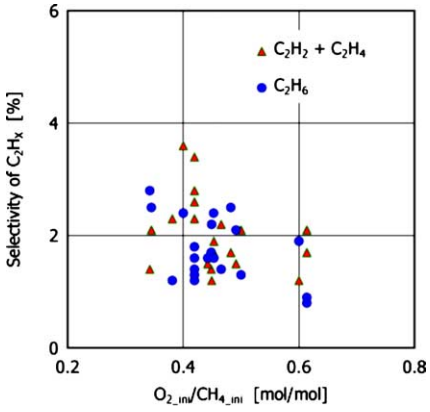

Fig. 8. Selectivity of C2 hydrocarbons.

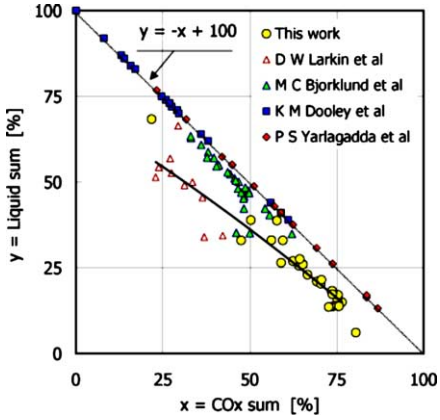

Fig. 9. CO_X vs. liquid sum. DBD: this work and Larkin et al. [21], thermal reaction: Bjorklund et al. [7], Dooley and co-workers [5], and Yarlagadda et al. [30].

yield of oxygenates [7], but such a process requires a rather complicated system. Non-thermal plasma reaches higher methane conversion at ambient temperature, but its selectivity is not as high as in the thermochemical method: there is a clear trade-off between methane conversion and selectivity of oxygenates.

4.3. Byproducts

In addition to oxygenates and CO_X, different types of hydrocarbons were produced through low-temperature plasma catalysis. Fig. 8 shows a plot of selectivity of C_2 hydrocarbon with respect to initial O_2/CH_4 ratios. Ethane and acetylene were not shown as separate by GC. Selectivity of C_2 hydrocarbon was no more than 6% overall, and it increases with decreasing initial O_2/CH_4 ratio. Generally, ethane will be the main product among C_2 hydrocarbons when methane is processed by DBD [31] because coupling of CH_3 (R4) is most likely to happen along with several chain reactions (R2 and R3) [32].

$$CH_4 + e \rightarrow CH_3 + H + e \quad \text{(R1)}$$

$$CH_4 + H \rightarrow CH_3 + H_2 \quad \text{(R2)}$$

$$CH_4 + CH_4^+ \rightarrow CH_3 + CH_5^+ \quad \text{(R3)}$$

$$CH_3 + CH_3 \rightarrow C_2H_6^* \rightarrow C_2H_6(+M) \quad \text{(R4)}$$

However, selectivity of ethane is comparable to other C_2 components because CH_3 produces various oxygenates other than C_2H_6 in the presence of oxygen. Selectivity of oxygenates is plotted with respect to selectivity of CO_X (Fig. 9). All data points referred from thermochemical reactions come on a single line, which is expressed by the following relation.

$$(\%\text{selectivity of liquid sum}) = 100 - (\%\text{selectivity of } CO_X) \quad (6)$$

Eq. (6) shows that the main products of the thermochemical reaction are organic oxygenates and CO_X. Generally, selectivity of CO_X will increase with initial oxygen content, whereas a methane rich condition will yield organic liquids: C_2 hydrocarbon will not be produced in a thermal reaction system. On the other hand, selectivity of liquid oxygenates in DBD is slightly lower than in the thermochemical reaction results because low-temperature plasma catalysis produces C_2 hydrocarbons. If the O_2/CH_4 ratio becomes much lower than 0.5, C_2 hydrocarbons and yellowish compounds are formed. Consequently, all data decrease far below the line. Methane tends to polymerize in oxygen-poor conditions. Another particular characteristic of DBD is the production of relatively large amounts of H_2. Fig. 10 shows selectivity of CO and the H_2/CO ratio with respect to the initial O_2/CH_4 ratio. Although the H_2/CO ratio slightly decreases with initial O_2/CH_4 ratio, it is approximately unity. The remaining syngas, which includes large amounts of CO (50% selectivity) might be converted to oxygenate with an appropriate post process. Unique reaction characteristics of low-temperature plasma catalysis will be discussed further in relation to numerical simulation of microdischarge.

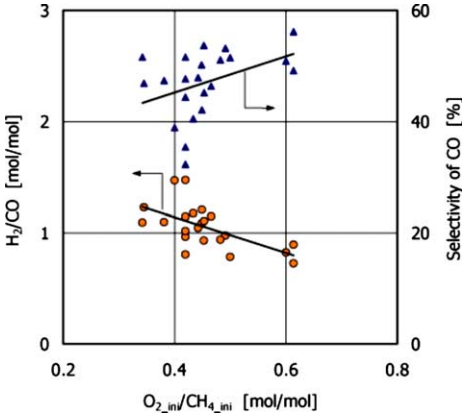

Fig. 10. The H_2/CO ratio and selectivity of CO for the initial O_2/CH_4 ratio.

5. Reaction mechanism

5.1. Numerical simulation of microdischarge and related chemistry

In general, partial oxidation of methane starts with CH_3 production, followed by several chain reactions as long as thermal reaction governs the production of oxygenates [33].

$$CH_4 \rightarrow CH_3 + H \quad \text{(R5)}$$

$$CH_3 + O_2 \rightarrow CH_3OO \quad \text{(R6)}$$

$$CH_3OO + CH_3 \rightarrow 2CH_3O \quad \text{(R7)}$$

$$CH_3O + CH_4 \rightarrow CH_3OH + CH_3 \quad \text{(R8)}$$

A unique feature of low-temperature plasma is that at least four different types of radicals are shown to be produced simultaneously by electron swarm, which is a group of electrons having a wide distribution of energies: the impact of high-energy electrons creates excited methane for which the internal excited energy (9–12 eV) is much higher than the dissociative threshold (4.26 eV).

$$\begin{aligned} CH_4 + e &\rightarrow CH_4(s) + e \rightarrow CH_3 + H + e \\ &\rightarrow CH_2 + H_2 + e \\ &\rightarrow CH + H + H_2 + e \\ &\rightarrow C + 2H_2 + e \end{aligned} \quad (7)$$

In general, the average electron energy in DBD does not become higher than 10 eV. However, some electrons that have higher energy than the dissociative threshold are able to decompose gaseous molecules. Our numerical results show that the average electron energy becomes 6.5 eV when external field strength corresponds to 300 Td. Moreover, 24% of all electrons have energy that is higher than the 9 eV necessary to dissociate methane; 8% of electrons have energy higher than the 12.6 eV that is necessary to ionize methane (CH_4^+). A small number of high-energy electrons play a major role in the generation of secondary electrons: this phenomenon is called electron avalanche. Therefore, electron swarm with an average energy of 6.5 eV is sufficient to decompose and ionize methane molecules. In the same way, the fragmentation pattern of CH_i ($i = 0$–3) radicals depends not only on the collision cross section of methane, but also on the electron energy distribution function (EEDF) in given conditions. Melton and Rudolph [34] reported that the fragmentation pattern of methane in low-pressure RF capacitive discharge is:

$$\begin{aligned} CH_4 + e \rightarrow\ & CH_3(80\%),\ CH_2(13.3\%), \\ & CH(6.7\%),\ C(0.006\%). \end{aligned} \quad (8)$$

Nakano et al. [35] also inferred that CH_3 and CH_2 are the main fragments in low-pressure RF discharge with a similar distribution rate. On the contrary, atmospheric pressure plasma must consider all four fragments because electron energy is higher than that of low-pressure RF discharges. In fact, a collision cross-section of methane shows four distinctive cross sections of methane fragmentation. We considered all cross section data in modeling and performed numerical simulation of streamer propagation and related elementary reactions, as shown in Fig. 11 [15]. The detailed reaction mechanism whereby a methane and oxygen mixture interacts with electrons remains unclear. However, we simulated streamer formation in pure methane to elucidate the fragmentation pattern of methane by electron impact. For simplicity, numerical analysis excludes the polymerization process. According to Fig. 11(a), electron and CH_i ($i = 0$–3) fragments, including atomic H, increase equally as a streamer propagates. In the absence of oxygen, atomic H reacts quickly with atomic H to form H_2: atomic H does not contribute to hydrogen abstraction from CH_i radicals ($i = 1$–4). In fact, Fig. 11 shows that densities of C, CH, and CH_2 decrease much faster than H as soon as the streamer is terminated. Density of CH_3 is much higher than other fragments because hydrogen abstraction by CH_4^+ ion (R3) continues to produce CH_3, which subsequently produces C_2H_6 via R4: atomic H does not appear to promote further methane fragmentation. Consequently, C_2H_6 becomes the main product, whereas concentration of C_2H_2 and C_2H_4 is one order of magnitude lower than C_2H_6. Fig. 12 represents a fragmentation pattern as a function of an external electric field calculated by ELENDIF software, which solves the time dependent electron energy distribution function using a two-term spherical harmonic expansion solutions of the

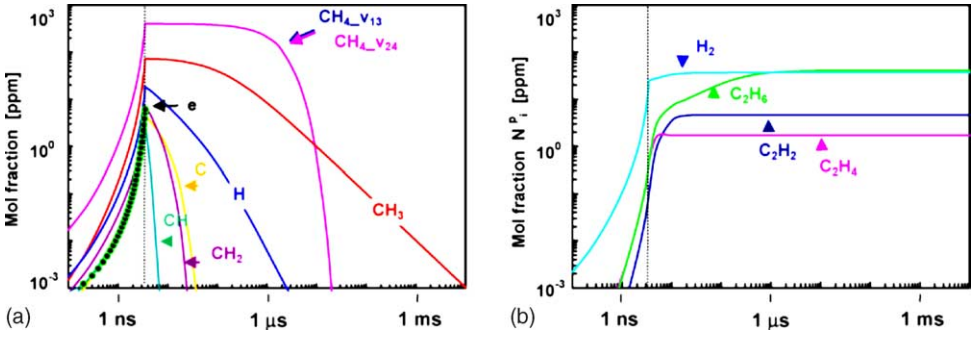

Fig. 11. Evolution of a streamer at 300 K–100 kPa and 200 Td: (a) electron and radicals; (b) final products.

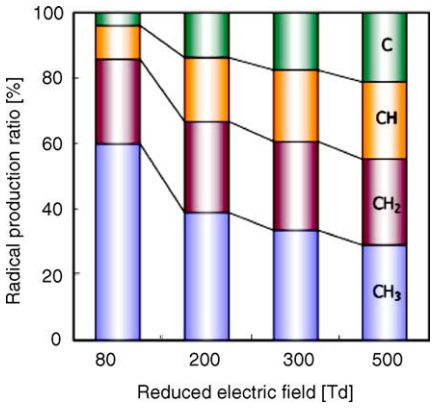

Fig. 12. Fragmentation pattern of CH_i radicals ($i = 0$–3) by electron impact of CH_4.

Boltzmann transport equation [36]. Swarm parameters derived from solutions show good agreement when reduced field strength is lower than 500 Td [37,38]. Dissociation to CH_3 will increase with decreasing electric field. It reaches 60% when the external field corresponds to a breakdown field of methane (80 Td). Those CH_3 radicals are considered to react with oxygen related radicals to produce various oxygenates. Maximum selectivity of 60% might be obtained at the lowest electric field. However, the discharge current decreases markedly, concomitant with a decrease in the external field. Fig. 13 shows a nanosecond current pulse generated by a single microdischarge. When the external field corresponds to 200 Td, the streamer bridges the gas gap in 3.5 ns; thereby, peak current reaches 50 mA. On the other hand, the streamer traverses the gap much more rapidly at 300 Td and the peak current becomes four times higher than that of 200 Td. Application of a stronger electric field is desirable to increase methane conversion, but selectivity of oxygenates will decrease as the external electric field increases.

It is noteworthy that CH_2, CH, and C are also generated during streamer propagation. Those radicals ultimately produce CO_X instead of oxygenates. A salient problem is that those radicals seem not to pass through oxygenates:

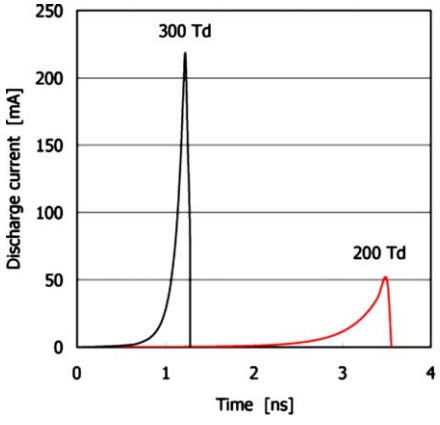

Fig. 13. Nanosecond current pulse of streamer formation.

production of CO_X is unavoidable even if the initial O_2/CH_4 ratio is minimized. Selectivity of a product by non-thermal plasma catalysis is hard to control unless the electron energy distribution function does change. This fact indicates that the selectivity of oxygenates does not change greatly with respect to methane conversion and the initial O_2/CH_4 ratio (see Figs. 6 and 10, respectively). In addition, the selectivity of C_2H_6 is comparable to that of $C_2H_2 + C_2H_4$ in the presence of oxygen (see Fig. 8), suggesting that an original CH_3 fragment that is produced by electron impact during streamer propagation will react with oxygen to produce oxygenates rather than C_2H_6. In contrast, CH_j ($j = 0$–2) radicals will not produce oxygenates like methanol. They will more likely generate CO_X. Selectivity of oxygenates depends strongly on the initial fragmentation pattern of methane.

5.2. Gas temperature of filamentary microdischarge

We used emission spectroscopy to measure the rotational temperature of CH (431.5 nm). Emission spectroscopy reasonably represents plasma gas tempera-ture of the corresponding emission region. Thermal relaxation of excited CH is established by molecular collision within a radiative lifetime (1–5 ns). Thereby, the rotational temperature can be derived by the Boltzmann plot method. Detailed procedures of determining the rotational temperature and its availability have been discussed in detail by Nozaki et al. [16,39–41]. The rotational temperature is plotted in Fig. 14 with respect to the O_2/CH_4 ratio.

The rotational temperature was 200 °C higher than the temperature of the heat reservoir even though $O_2/CH_4 = 0$. In general, the discharge filament temperature is 100–300 °C higher than the average gas temperature. This means that the temperature increase is caused by the heat

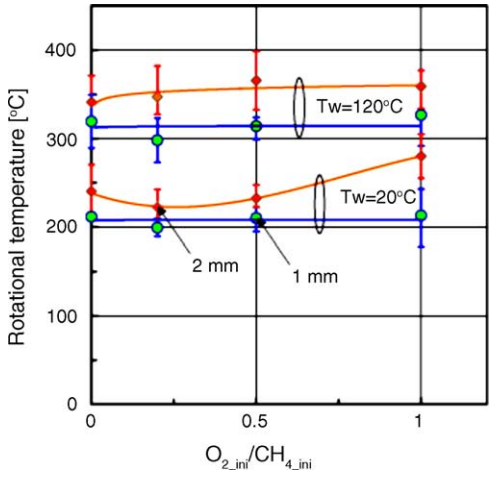

Fig. 14. Rotational temperature that corresponds to gas temperature of developing microdischarges. Reactor wall temperature $T_w = 20$ °C and 120 °C, and reactor size: 1 mm (●) and 2 mm (◆). Discharge power (3–10 W) >heat released by partial oxidation (<1 W).

produced by barrier discharge. In fact, rotational temperature does not increase with increased O_2 content. Heat that is released by partial oxidation does not contribute to a temperature increase in the reaction field. Nevertheless, heat seemed to increase slightly in this case when the glass diameter was 2 mm. When wall temperature increased from 20 to 120 °C, the rotational temperature also increased an additional 100 °C. Nevertheless, the rotational temperature was still sufficiently low that it did not initiate thermal reactions. Production of acetylene does not necessarily indicate that the gas temperature is extremely high (e.g. ca. 1000 °C) because the inelastic electron impact can produce various radicals which eventually form acetylene, even at room temperature. If the gas temperature were increased markedly by plasma, the main product among C_2 compounds would become acetylene, with much higher selectivity than that shown in this experiment. As discussed in Section 4.1 (see Eq. (5)), a high-frequency power source is strongly desired for operation of micro-plasma reactors: it would markedly decrease the residence time in a miniaturized reactor. However, high frequency operation seems to increase the reaction temperature unexpectedly, simply because the energy density also increases with frequency. The reactor dimension and operating frequency must be optimized to create an ideal excitation and quenching environment, which is desirable for efficient partial oxidation of methane.

6. Concluding remarks

Partial oxidation of methane was investigated using microscale dielectric barrier discharge reactor. General characteristics were compared to those obtained from a conventional thermochemical reaction system. A reaction mechanism was also discussed based on numerical simulation and spectroscopic measurement of a microscale barrier discharge reactor. The authors conclude that the one-pass methanol yield exceeded 10%. It even reached 17%, as shown in Table 2, when the reaction temperature and residence time were selected appropriately. However, the present micro-plasma reactor must be modified for stable operation. Liquid oxygenates that include water vapor quickly condense and plug the glass capillary, causing unstable pulsating flow. Because of this problem, liquid oxygenates seemed to remain in the capillary for a much longer time than the calculated residence time, engendering further decomposition of oxygenates. It reached 17% yield within reasonable measurement error, but that is not an averaged value. Currently, we assert that 10% is the maximum reasonably reproducible yield.

1. The flow-type, microscale, non-equilibrium plasma generated within this extremely confined environment realized 10% one-pass methanol yield at 25 °C and 100 kPa within 280 ms. The CH_4/O_2 mixture was processed without dilution or explosion.
2. A salient advantage of low-temperature plasma catalysis of methane is that the least reactive methane is activated by high-energy electron impacts almost independently of temperature and pressure. Thereby, 40% methane conversion is achieved. That conversion is four times higher than that of a thermochemical reaction system.
3. Unlike thermochemical reactions, product selectivity is almost independent of methane conversion unless the methane fragmentation pattern changes.
4. Excess oxygen tends to yield CO_X rather than oxygenates. On the other hand, a relatively large amount of C_2 hydrocarbons (C_2H_2, C_2H_4, and C_2H_6: 6 vol% in total) are produced independently of the initial O_2/CH_4 ratio.
5. C, CH, CH_2, and CH_3 are shown to be produced simultaneously by electron swarm. CH_3 seems to produce oxygenates rather than C_2H_6 in the presence of oxygen, whereas CH_j ($j = 0$–2) radicals produce CO_X directly with no production via oxygenates. Selectivity of oxygenates depends more on the initial fragmentation pattern of methane.
6. The highest selectivity of oxygenates (ca. 60%), which is related to the production of CH_3, might be obtained when external electric field corresponds to the breakdown field of methane. Stronger electric fields engender higher methane conversion rates because the discharge current increases markedly. Nevertheless, selectivity of oxygenates decreases at higher field strength.
7. General characteristics of micro-plasma reactors are similar to those of conventional barrier discharge reactors (e.g. Figs. 6,7 and 9) because the initial feedstock (O_2/CH_4 ratio) and electron energy distribution seems not to have changed too much. One major difference is that methanol selectivity in the micro-plasma reactor is much higher than in other oxygenates. Fist of all, the discharge space in a micro-plasma reactor is confined both radially and laterally to enhance the quenching effect. Second, the production rate of oxygenates is presumed to be much faster in a micro-plasma reactor because of high frequency operation. This situation increases the partial pressure of oxygenates, leading to efficient condensation of liquid products, including water vapor, in the reactor. If the partial pressure of oxygenates is much lower than the vapor pressure at a given condition, further oxidation of oxygenates is likely to occur in the gas phase.
8. The best result achieved in this study (see Table 2 row a) showed that the energy requirement to produce 1 kg of methanol corresponded to 69 kWh kg^{-1}, which implies a methanol production cost of US$5–US$6/kg where the electric power charge was assumed to be $0.07–$0.09/kWh. In marked contrast, the methanol production cost by the methane steam reforming technique is about $0.2/kg. At the moment, the micro-plasma reactor we have proposed is not compatible with existing multi-stage methanol and formaldehyde manufacturing processes.

9. Gas temperature of microdischarges was 200 °C higher than the wall temperature because microdischarges are localized in a narrow filamentary region. A high-frequency power source is important for operation of a micro-plasma reactor, but it seems to increase plasma gas temperature unexpectedly high because the power density also increases with frequency. The reactor dimension and operating frequency must be optimized for the best environment, which offers a combination of excitation and quenching.

Acknowledgement

Authors would like to thank Dr. Shigeru Kado for intensive discussion.

References

[1] P.S. Casey, T. McAllister, K. Foger, Ind. Eng. Chem. Res. 33 (1994) 1120.
[2] K. Omata, N. Fukuoka, K. Fujimoto, Ind. Eng. Chem. Res. 33 (1994) 784.
[3] K. Otsuka, Y. Wang, Appl. Catal. A Gen. 222 (2001) 145.
[4] N.R. Hunter, H.D. Gesser, L.A. Morton, P.S. Yarlagadda, Appl. Catal. 57 (1990) 45.
[5] W. Feng, F.C. Knopf, K.M. Dooley, Energy Fuels. 8 (1994) 815.
[6] R.A. Periana, D.J. Taube, S. Gamble, H. Taube, T. Satoh, H. Fuji, Science 280 (1998) 560.
[7] M.C. Bjorklund, R.W. Carr, Ind. Eng. Chem. Res. 41 (2002) 6528.
[8] W.C. Danen, M.J. Ferris, J.L. Lyman, R.C. Oldenborg, C.K. Rofer, G.E. Steit, Petro. Chem. Div. 36 (1991) 166, Preprints, Published by ASC.
[9] Y. Sekine, K. Fujimoto, Energy Fuels 10 (1996) 1278.
[10] T. Nozaki, A. Hattori, S. Kado, K. Okazaki, in: Proceedings of the Third International Workshop on Basic Aspects of Non-equilibrium Plasmas Interacting with Surfaces, 1, 2003, p. 8.
[11] T. Nozaki, S. Kado, A. Hattori, K. Okazaki, N. Muto, Natural gas conversion VII, in: X. Bao, Y. Xu (Eds.) Proceedings of 7th Natural Gas Conversion Symposium, vol. 147, Dalian, China, June 6–10, 2004, Studies in Surface Science and Catalysis, pp. 505–510.
[12] U. Kogelschatz, Plasma Chem. Plasma Process. 23 (1) (2003) 1–46.
[13] K. Okazaki, T. Kishida, K. Ogawa, T. Nozaki, Energy Convers. Manage. 43 (2002) 1459–1468.
[14] K. Okazaki, T. Nozaki, Pure Appl. Chem. 74 (3) (2002) 447–452.
[15] T. Nozaki, N. Muto, S. Kado, K. Okazaki, Catal. Today 89 (2004) 57–65.
[16] T. Nozaki, N. Muto, S. Kado, K. Okazaki, Catal. Today 89 (2004) 67–74.
[17] L.M. Zhou, B. Xue, U. Kogelschatz, B. Eliasson, Energy Fuel 12 (1998) 1191–1199.
[18] T. Hammer, T. Kappes, W. Schiene, ACS Symposium Series No. 852, 2002, pp. 292–301.
[19] H. Kabashima, H. Einaga, S. Futamura, IEEE Trans. Ind. Appl. 39 (2) (2003) 340–345.
[20] J.G. Wang, C.J. Liu, B. Elaisson, Energy Fuels 18 (1) (2004) 148–153.
[21] D.W. Larkin, L.L. Lobban, R.G. Mallinson, Catal. Today 71 (2001) 199.
[22] B. Lewis, Combustion, Flames and Explosions of Gases, Academic Press, Inc, 1987.
[23] von Engel, Ionized Gases, Oxford University Press, 1965.
[24] G. Herzberg, Molecular Spectra and Molecular Structure, London, 1950, p. 32.
[25] N. Gherardi, S. Martin, F. Massines, J. Phys. D: Appl. Phys. 33 (2000) 104.
[26] E. Francke, S. Robert, J. Amouroux, High Temp. Mater. Processes 4 (2000) 139–150.
[27] Y. Moro-oka, Catal. Today 45 (1998) 3–12.
[28] A. Vincent, F. Daou, J. Amouroux, High Temp. Mater. Processes 6 (2002) 167–180.
[29] S. Kado, K. Urasaki, Y. Sekine, K. Fujimoto, T. Nozaki, K. Okazaki, Fuel 82 (2003) 2291–2297.
[30] P.S. Yarlagadda, L.A. Morton, N.R. Huntera, H.D. Gesser, Ind. Eng. Chem. Res. 27 (1988) 252–256.
[31] S. Kado, Y. Sekine, T. Nozaki, K. Okazaki, Catal. Today 89 (2004) 47–55.
[32] K. Tachibana, M. Nishida, H. Harima, Y. Urano, J. Phys. D: Appl. Phys. 17 (1984) 1727–1742.
[33] O.V. Krylov, Catal. Today 18 (1993) 209–302.
[34] C.E. Melton, P.S. Rudolph, J. Chem. Phys. 47 (1967) 1771–1774.
[35] T. Nakano, H. Toyoda, H. Sugai, Jpn. J. Appl. Phys. 30 (19912912).
[36] W.L. Morgan, Plasma Chem. Plasma Process. 12 (4) (1992) 477–493.
[37] J. Davies, C.J. Evans, F. Llewellyn Jones, Proc. R. Soc. London Ser. A 281 (1964) 164–183.
[38] Y. Ohmori, K. Kitamori, M. Shimozuma, H. Tagashira, J. Phys. D: Appl. Phys. 19 (1986) 437–455.
[39] T. Nozaki, Y. Unno, Y. Miyazaki, K. Okazaki, J. Phys. D: Appl. Phys. 34 (2001) 2504.
[40] T. Nozaki, Y. Miyazaki, Y. Unno, K. Okazaki, J. Phys. D: Appl. Phys. 34 (2001) 3383.
[41] T. Nozaki, Y. Unno, K. Okazaki, Plasma Sources Sci. Technol. 11 (2002) 431.